Feedback Systems

An Introduction for Scientists and Engineers

SECOND EDITION

Karl Johan Åström
Richard M. Murray

Version v3.0j (2019-08-18)

This is the electronic edition of *Feedback Systems* and is available from http://fbsbook.org. Hardcover editions may be purchased from Princeton University Press, http://press.princeton.edu/titles/8701.html.

Chapter Thirteen

Robust Performance

However, by building an amplifier whose gain is deliberately made, say 40 decibels higher than necessary (10000 fold excess on energy basis), and then feeding the output back on the input in such a way as to throw away the excess gain, it has been found possible to effect extraordinary improvement in constancy of amplification and freedom from non-linearity.

Harold S. Black, "Stabilized Feedback Amplifiers," 1934 [Bla34].

This chapter focuses on the analysis of robustness of feedback systems, a vast topic for which we provide only an introduction to some of the key concepts. We consider the stability and performance of systems whose process dynamics are uncertain. We make use of generalizations of Nyquist's stability criterion as a mechanism to characterize *robust* stability and performance. To do this we develop ways to describe uncertainty, both in the form of parameter variations and in the form of neglected dynamics. We also briefly mention some methods for designing controllers to achieve robust performance.

13.1 MODELING UNCERTAINTY

Harold Black's quote above illustrates that one of the key uses of feedback is to provide robustness to uncertainty ("constancy of amplification"). It is one of the most useful properties of feedback and is what makes it possible to design feedback systems based on strongly simplified models. In this section we explore different types of uncertainty in our knowledge of the dynamics of the system, including the important problem of determining when two systems are similar from a controls perspective.

Parametric Uncertainty

One form of uncertainty in dynamical systems is *parametric uncertainty* in which the parameters describing the system are not precisely known. A typical example is the variation of the mass of a car, which changes with the number of passengers and the weight of the baggage. When linearizing a nonlinear system, the parameters of the linearized model also depend on the operating conditions. It is straightforward to investigate the effects of parametric uncertainty simply by evaluating the performance criteria for a range of parameters. Such a calculation reveals the consequences of parameter variations. We illustrate by an example.

Example 13.1 Cruise control
The cruise control problem is described in Section 4.1, and a PI controller was designed in Example 11.3. To investigate the effect of parameter variations, we

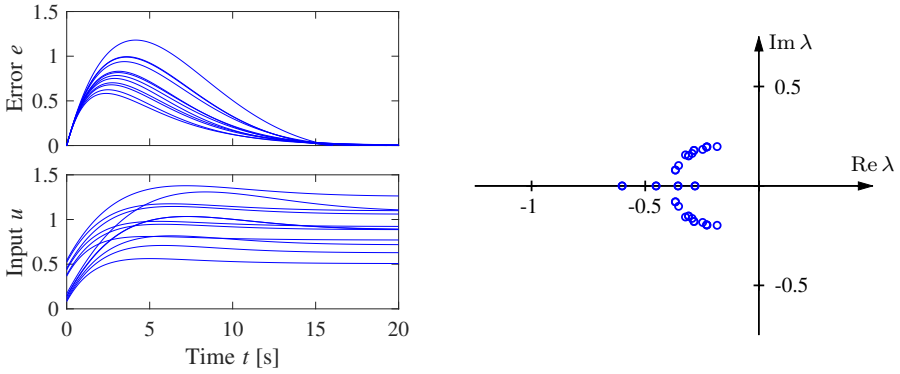

(a) Disturbance response (b) Closed loop eigenvalues

Figure 13.1: Responses of the cruise control system to a slope increase of 4° (a) and the eigenvalues of the closed loop system (b). Model parameters are swept over a wide range. The closed loop system is of second order.

will choose a controller designed for a nominal operating condition corresponding to mass $m = 1600$ kg, fourth gear ($\alpha = 12$), and speed $v_e = 20$ m/s; the controller gains are $k_p = 0.5$ and $k_i = 0.1$. Figure 13.1a shows the velocity error e and the throttle u when encountering a hill with a 4° slope with masses in the range $1600 < m < 2000$ kg, gear ratios 3–5 ($\alpha = 10$, 12, and 16), and velocity $10 \leq v \leq 40$ m/s. The simulations were done using models that were linearized around the different operating conditions. The figure shows that there are variations in the response but that they are all quite reasonable. The largest velocity error is in the range of 0.5–1.2 m/s, and the settling time is about 15 s. The control signal is larger than 1 in some cases, which implies that the throttle is fully open. (A full nonlinear simulation using a controller with windup protection is required if we want to explore these cases in more detail.) The closed loop system has two eigenvalues, shown in Figure 13.1b for the different operating conditions. We see that the closed loop system is well damped in all cases. ∇

This example indicates that at least as far as parametric variations are concerned, a design based on a simple nominal model will give satisfactory control. The example also indicates that a controller with fixed parameters can be used in all cases. Notice that we have not considered operating conditions in low gear and at low speed, but cruise controllers are not typically used in these cases.

Unmodeled Dynamics

It is generally easy to investigate the effects of parametric variations. However, there are other uncertainties that also are important, as discussed at the end of Section 3.1. The simple model of the cruise control system captures only the dynamics of the forward motion of the vehicle and the torque characteristics of the engine and transmission. It does not, for example, include a detailed model of the engine dynamics (whose combustion processes are extremely complex) or the slight delays that can occur in modern electronically-controlled engines (as a result of the processing time of the embedded computers). These neglected mechanisms are called *unmodeled dynamics*.

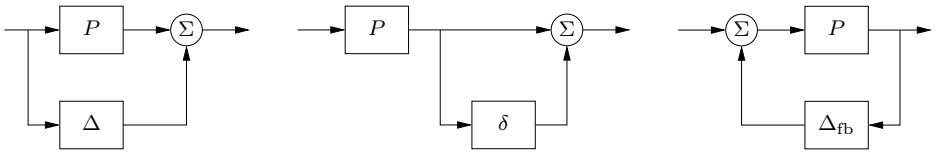

(a) Additive uncertainty (b) Multiplicative uncertainty (c) Feedback uncertainty

Figure 13.2: Unmodeled dynamics in linear systems. Uncertainty can be represented using additive perturbations (a), multiplicative perturbations (b), or feedback perturbations (c). The nominal system is P, and Δ, δ, and Δ_{fb} represent unmodeled dynamics.

One way to account for unmodeled dynamics is by developing a more complex model that includes additional details that are deemed important for control design. Such models are commonly used for controller development, but substantial effort is required to generate them. In addition, these models are themselves likely to be uncertain, since the parameter values may vary over time or between units. Performing parametric analysis on complex models can be very time-consuming, especially if the parameter space is large.

An alternative is to investigate if the closed loop system can be made insensitive to generic forms of unmodeled dynamics. The basic idea is to augment the nominal model with a bounded input/output transfer function that captures the gross features of the unmodeled dynamics. For example, in the cruise control example the model of the engine can be a static model that provides the torque instantaneously and the augmented model can include a time delay with an unknown but bounded value. Describing unmodeled dynamics with transfer functions permits us to handle infinite dimensional systems like time delays.

Figure 13.2 illustrates some ways in which unmodeled dynamics can be captured. The transfer functions Δ, δ, Δ_{fb} are taken as bounded input/output operators that represent the unmodeled dynamics. For example, in Figure 13.2a we assume that the transfer function of the process is $\tilde{P}(s) = P(s) + \Delta(s)$, where $P(s)$ is the nominal simplified transfer function and $\Delta(s)$ is a transfer function that represents the unmodeled dynamics in terms of *additive uncertainty*. If we can show that the closed loop system is stable for all $\Delta(s)$ satisfying a given bound (e.g., $|\Delta(s)| < \epsilon$), then the system is said to be *robustly stable*.

Different representations are possible in addition to additive uncertainty. Figure 13.2b shows a representation for *multiplicative uncertainty* and Figure 13.2c represents *feedback uncertainty*. The specific form that is used depends on what provides the best representation of the unmodeled dynamics. The different types of uncertainty can also be related to each other:

$$\delta = \frac{\Delta}{P}, \qquad \Delta_{\text{fb}} = \frac{\Delta}{P(P+\Delta)} = \frac{\delta}{P(1+\delta)}.$$

We will return to these representations in the next section, where we develop conditions for robust stability in the presence of unmodeled dynamics.

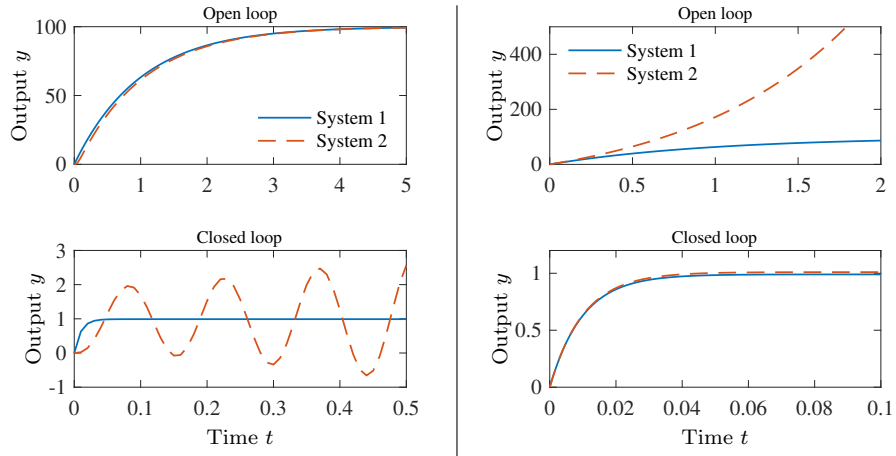

(a) Example 13.2 (b) Example 13.3

Figure 13.3: Determining when two systems are close. The plots in (a) show a situation when the open loop responses are almost identical, but the closed loop responses are very different. The processes are given by equation (13.1) with $k = 100$ and $T = 0.025$. The plots in (b) show the opposite situation: the systems are different in open loop but similar in closed loop. The processes are given by equation (13.3) with $k = 100$.

When Are Two Systems Similar?

A fundamental issue in describing robustness is to determine when two systems are close. Given such a characterization, we can then attempt to describe robustness according to how close the actual system must be to the model in order to still achieve the desired levels of performance. This seemingly innocent problem is not as simple as it may appear. A naive approach is to say that two systems are close if their open loop responses are close. Even if this appears natural, there are complications, as illustrated by the following examples.

Example 13.2 Systems similar in open loop but different in closed loop
The systems with the transfer functions

$$P_1(s) = \frac{k}{s+1}, \qquad P_2(s) = \frac{k}{(s+1)(sT+1)^2} \tag{13.1}$$

have very similar open loop step responses for small values of T, as illustrated in the upper plot in Figure 13.3a, which is plotted for $T = 0.025$ and $k = 100$.

The differences between the open loop step responses are barely noticeable in the figure. Closing a feedback loop with unit gain ($C = 1$) around the systems gives closed loop systems with the transfer functions

$$T_1(s) = \frac{k}{s+1+k}, \quad T_2(s) = \frac{k}{s^3T^2 + (T^2+2T)s^2T + (1+2T)s + 1 + k}. \tag{13.2}$$

We find that T_1 is stable for $k > -1$ and T_2 is stable for $-1 < k < 2T + 4 + 2/T$. With the numerical values $k = 100$ and $T = 0.025$ the transfer function T_1 is stable and T_2 is unstable, which is clearly seen in the closed loop step responses in the

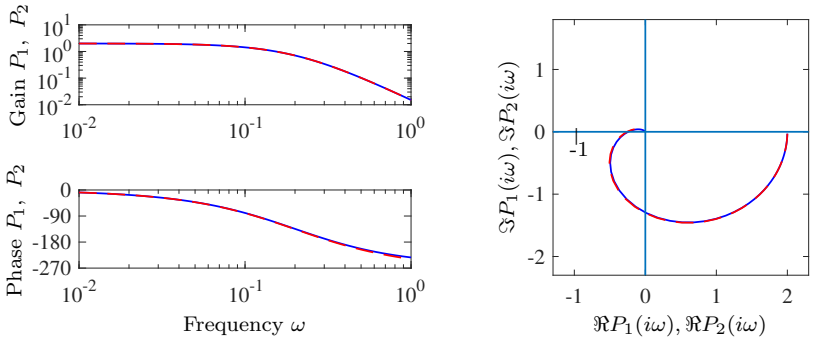

(a) Bode plot (b) Nyquist plot

Figure 13.4: Comparison of frequency response of $P_1(s)$ (solid) and $P_2(s)$ (dashed). (a) Bode plot and (b) Nyquist plot.

lower plot in Figure 13.3a. ∇

Example 13.3 Systems different in open loop but similar in closed loop
Consider the systems

$$P_1(s) = \frac{k}{s+1}, \qquad P_2(s) = \frac{k}{s-1}. \tag{13.3}$$

The open loop responses are different because P_1 is stable and P_2 is unstable, as shown in the upper plot in Figure 13.3b. Closing a feedback loop with unit gain ($C = 1$) around the systems, we find that the closed loop transfer functions are

$$T_1(s) = \frac{k}{s+k+1}, \qquad T_2(s) = \frac{k}{s+k-1}, \tag{13.4}$$

which are very close for large k, as shown in the lower plot in Figure 13.3b. ∇

The examples we have just discussed indicate that comparing time responses may not be a good way to compare systems. We will next compare frequency responses.

Example 13.4 Comparison of systems via frequency responses
Consider the systems

$$P_1(s) = \frac{2}{(1+5s)^3(1-0.05s)}, \qquad P_2(s) = \frac{2}{(1+5s)^3(1+0.05s)}. \tag{13.5}$$

Bode and Nyquist plots of these transfer functions are shown in Figure 13.4. The figure shows that both systems have very similar Bode and Nyquist plots. In spite of this, the closed loop systems obtained with unit feedback are very different. Neither system has any zeros, but P_1 has two poles in the left half-plane and one pole in the right half-plane while P_2 has all its poles in the left half-plane. Both $1 + P_1$ and $1 + P_2$ have winding number $n_{\mathrm{w}} = 0$. Since P_1 has a pole in the right half-plane it follows from the Nyquist criterion (Theorem 10.3) that the characteristic polynomial of the closed loop system obtained with unit feedback has one zero in the right half-plane ($f = 1 + P_1$, $n_{\mathrm{z},D} = n_{\mathrm{w},\Gamma} + n_{\mathrm{p},D}$ in the principle of variation of the argument, Theorem 10.2). Thus the closed loop system using P_1 is unstable

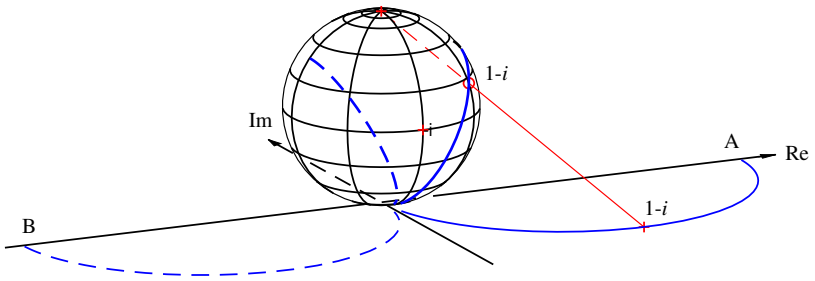

Figure 13.5: Geometric interpretation of the chordal metric $d(P_1, P_2)$ on a Nyquist plot with a Riemann sphere. At each frequency, the points on the Nyquist curve for P_1 (solid, starting at A) and P_2 (dashed, starting at B) are projected onto the sphere of diameter 1 positioned at the origin of the complex plane. The projection of the point $1 - i$ is shown in the figure. The distance between the two systems is defined as the maximum distance between the projections of $P_1(i\omega)$ and $P_2(i\omega)$ over all frequencies ω. The figure is plotted for the transfer functions $P_1(s) = 2/(s + 1)$ and $P_2(s) = 2/(s - 1)$. (Diagram courtesy G. Vinnicombe.)

while the closed loop system using P_2 is stable. ∇

The important lesson to learn from this example is that two systems may not be close from the point of view of feedback even if their open loop frequency responses are similar. It is also necessary that both systems satisfy the winding number condition.

The Vinnicombe Metric

Examples 13.2 and 13.3 show that comparing open loop time responses is not a good way to judge closed loop behavior. Example 13.4 shows that it is necessary to have a winding number condition if frequency responses are compared. We will now introduce the *Vinnicombe metric*, which is the proper way to compare open loop systems in a way that reflects their closed loop behavior. The metric is closely related to the Nyquist plot; more information is available in [Vin93, Vin01].

We start by introducing the *chordal metric*, which is a function $\mathbb{C} \times \mathbb{C} \to [0\ 1]$ that maps two complex numbers to a real variable in the range $0 \leq x \leq 1$. Applied to the transfer functions $P_1(s)$ and $P_2(s)$ the chordal metric is defined as

$$d_{P_1 P_2}(\omega) := \frac{|P_1(i\omega) - P_2(i\omega)|}{\sqrt{1 + |P_1(i\omega)|^2}\sqrt{1 + |P_2(i\omega)|^2}}. \tag{13.6}$$

The chordal metric $d_{P_1 P_2}$ has a nice geometric interpretation, illustrated in Figure 13.5. The points $P_1(i\omega)$ and $P_2(i\omega)$ are projected onto a sphere with diameter 1 positioned at the origin of the complex plane (the Riemann sphere). The projection is the intersection of the sphere with a straight line from the point to the north pole of the sphere (inverse stereographic projection). The chrodal distance is then the Euclidean distance between the two points on the sphere.

To define a metric between two transfer functions, Vinnicombe introduced the

following set $\mathcal{C}$ of rational transfer functions P_1 and P_2:

$$\mathcal{C} = \big\{P_1, P_2 : 1 + P_1(i\omega)P_2(-i\omega) \neq 0 \,\forall\, \omega, \\ n_{\mathrm{w},\Gamma}(1 + P_1(s)P_2(-s)) + n_{\mathrm{p,rhp}}(P_1(s)) - n_{\mathrm{p,rhp}}(P_2(-s)) = 0\big\}, \tag{13.7}$$

where $n_{\mathrm{w},\Gamma}(f)$ is the winding number for the function $f(s)$ around the Nyquist contour Γ and $n_{\mathrm{p,rhp}}(f)$ is the number of poles of the $f(s)$ in the open right half-plane. (Compare with the corresponding conditions in Nyquist's criterion in Theorem 10.3.) The metric is then defined as follows.

Definition 13.1 (The ν-gap metric)**.** Let $P_1(s)$ and $P_2(s)$ be rational transfer functions. The *ν-gap metric* is

$$\delta_\nu(P_1, P_2) = \begin{cases} \sup_\omega d_{P_1P_2}(\omega), & \text{if } (P_1, P_2) \in \mathcal{C}, \\ 1, & \text{otherwise,} \end{cases} \tag{13.8}$$

where $d_{P_1P_2}(\omega)$ is given by equation (13.6).

We will also call this metric the *Vinnicombe metric* after its inventor. Vinnicombe showed that $\delta_\nu(P_1, P_2)$ is indeed a metric. He extended it to multivariable and infinite dimensional systems, and he gave strong robustness results that will be discussed later. There is a MATLAB command `gapmetric` for computing the Vinnicombe metric.

Vinnicombe gave several interpretations of the winding number condition that determines if (P_1, P_2) belong to $\mathcal{C}$. He showed that the condition implies that the closed loop system obtained when $P_1(s)$ is connected in a feedback loop with $P_1(-s)$ has the same number of right half-plane poles as when $P_1(s)$ is connected with $P_2(-s)$. A necessary condition is that the rational functions $1 + P_1(s)P_1(-s)$ and $1 + P_1(s)P_2(-s)$ have the same number of zeros in the right half-plane. This condition can be interpreted as a continuity condition: the transfer function P can be continuously perturbed from P_1 to P_2 in such a way that there is no intermediate transfer function P where $d_{P_1P}(\omega) = 1$.

We illustrate the Vinnicombe metric by computing it for the systems in Examples 13.2 and 13.3.

Example 13.5 Vinnicombe metric for Example 13.2
The transfer functions P_1 and P_2 for the systems in Example 13.2 are given by equation (13.1). We have

$$f(s) = 1 + P_1(s)P_2(-s) = 1 + \frac{k^2}{(1 - s^2)(1 - sT)^2}, \quad k = 100.$$

The graph of $f(i\omega)$ for $-\infty \leq \omega \leq \infty$ is a closed contour in the right half-plane that does not encircle the origin (see Figure 13.6a and 13.6b for an enlargement of the region around the origin), hence $n_{\mathrm{w},\Gamma}(1 + P_1(s)P_2(-s)) = 0$. In addition, the transfer functions P_1 and P_2 have no poles in the right half-plane and we can conclude that $(P_1, P_2) \in \mathcal{C}$ (equation (13.7)). An alternative to verify the winding number condition is to compute the number of right half-plane zeros of the transfer functions $1 + P_1(s)P_1(-s)$ and $1 + P_1(s)P_2(-s)$. A direct computation shows that both transfer functions have one zero in the open right half-plane. It follows from equation (13.8) that the Vinnicombe metric is $\delta_\nu(P_1, P_2) = 0.89$, which is large

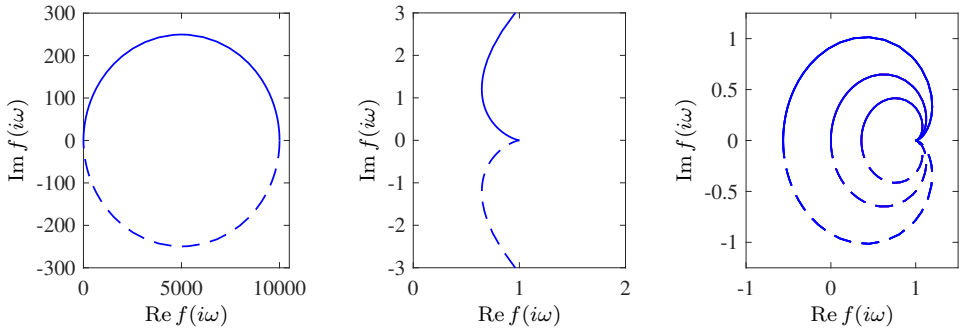

(a) Example 13.2 (b) Expansion of (a) near (0,0) (c) Example 13.3

Figure 13.6: Graphs of the function $f(i\omega) = 1 + P_1(i\omega)P_2(-i\omega)$ for $-\infty \leq \omega \leq \infty$. The plots for Example 13.2 with $P_1(s) = 100/(s+1)$ and $P_2(s) = 100/((s+1)(0.025s+1)^2$ are shown in (a), with an enlargement in the area close to the origin in (b). The plots for Example 13.3 with $P_1(s) = k/(s+1)$ and $P_2(s) = k/(-s+1)$ are shown in (c), with gains $k = 1.25$ (outer), $k = 1$, and $k = 0.8$ (inner). Values for positive ω are shown as solid lines and negative values are shown as dashed lines.

since 1.0 is as big as it can get, confirming that P_1 and P_2 are quite different. ∇

Example 13.6 Vinnicombe metric for Example 13.3
The transfer functions P_1 and P_2 for the systems in Example 13.3 are given by equation (13.3). We have

$$f_1(s) = 1 + P_1(s)P_1(-s) = 1 + \frac{k^2}{(1-s^2)} = \frac{-s^2 + 1 + k^2}{(1-s)^2},$$
$$f_2(s) = 1 + P_1(s)P_2(-s) = 1 - \frac{k^2}{(s+1)^2} = \frac{s^2 + 2s + 1 - k^2}{(s+1)^2}.$$

The rational function $f_1(s)$ has one zero in the right half-plane for all k, and the function $f_2(s)$ has a zero in the open right half-plane if $k > 1$. The winding number of $1 + P_1(s)P_2(-s)$ is 0 if $k \leq 1$ and 1 if $k > 1$, as seen in Figure 13.6c. Since P_1 has no poles in the right half-plane and P_2 has one pole in the right half-plane, equation (13.8) implies that $\delta_\nu(P_1, P_2) = 1$ if $k \leq 1$.

Another way to determine the winding number condition is to investigate if P_1 can be changed smoothly to P_2 without encountering points where $1+P_1(i\omega)P_2(i\omega) = 0$ (called conjugate points). To do so we introduce the transfer function $P_a(s) = k/(s+a)$, which changes smoothly from P_1 to P_2 as a changes from 1 to -1. We have

$$P_1(i\omega)P_a(-i\omega) = \frac{k^2}{(1+i\omega)(a-i\omega)} = \frac{k^2}{a + \omega^2 + i(a-1)\omega},$$

which implies that $P_1(0)P_a(0) = -1$ if $a = -k^2$. The points $P_1(0) = k$ and $P_a(0) = k/a = -1/k$ are thus conjugate points. Such points cannot be found if $k > 1$ because $a = -k^2$ would not be in the interval $-1 \leq a \leq 1$.

The transformation of $P_a(i\omega)$ from $P_1(i\omega)$ to $P_2(i\omega)$ can be visualized in Figure 13.5. From the previous analysis we know that it is sufficient to consider the case

$\omega = 0$. Assume $k \leq 1$. As a changes from 1 to 0, the point $P_a(0) = k/a$, marked A in Figure 13.5, moves along the positive real axis, from $P_1(0) = k$ towards infinity. The projection of $P_a(0)$ on the Riemann sphere moves along a meridian towards the north pole, which it reaches for $a = 0$. At that value the point flips from $P_{+0}(0) = \infty$ to $P_{-0}(0) = -\infty$, which both project onto the north pole. As a continues to decrease, the point $P_a(0)$ moves along the negative real axis from $-\infty$ to $-k$, and its projection on the Riemann sphere moves along a meridian from the north pole towards the south pole. For $a = -k^2$ we have $P_a(0) = -1/k$. The projection of this point is diametrically opposite the projection of $P_1(0) = k$ and the points have a chordal distance of 1 (the diameter of the sphere; see Exercise 13.4). Notice that a similar argument cannot be made when $k > 1$ because $|a| \leq 1$, and so the points k and k/a would both map to the upper hemisphere.

We have thus found that $(P_1, P_2) \in \mathcal{C}$ if $k > 1$, and equation (13.6) implies that

$$d_{P_1 P_2}(\omega) = \frac{2k}{1 + k^2 + \omega^2}.$$

The largest value occurs for $\omega = 0$, and the Vinnicombe metric, equation (13.8), becomes

$$\delta_\nu(P_1, P_2) = \begin{cases} 1 & \text{if } k \leq 1, \\ \dfrac{2k}{1 + k^2} & \text{if } k > 1. \end{cases}$$

With $k = 100$ we get $\delta_\nu(P_1, P_2) = 0.02$, which is a small number indicating that the transfer functions P_1 and P_2 are indeed very close. Figure 13.5 shows the Nyquist curves and their projections for $k = 2$, which gives $\delta_\nu(P_1, P_2) = 0.8$. ∇

13.2 STABILITY IN THE PRESENCE OF UNCERTAINTY

Having discussed how to describe uncertainty and the similarity between two systems, we now consider the problem of robust stability: when can we show that the stability of a system is robust with respect to process variations? This is an important question since the potential for instability is one of the main drawbacks of feedback. Hence we want to ensure that even if we have small inaccuracies in our model, we can still guarantee stability and performance of the closed loop system.

Robust Stability Using Nyquist's Criterion

The Nyquist criterion provides a powerful and elegant way to study the effects of uncertainty for linear systems. A simple criterion for a stable system is that the Nyquist curve be sufficiently far from the critical point -1. Recall that the shortest distance from the Nyquist curve to the critical point is $s_\mathrm{m} = 1/M_\mathrm{s}$, where M_s is the maximum of the sensitivity function and s_m is the stability margin introduced in Section 10.3. The maximum sensitivity M_s or the stability margin s_m is thus a good robustness measure, as illustrated in Figure 13.7a.

We will now derive explicit conditions on the controller C such that stability is guaranteed for process perturbations where $|\Delta|$ is less than a given bound. Consider a stable feedback system with a process P and a controller C. If the process is

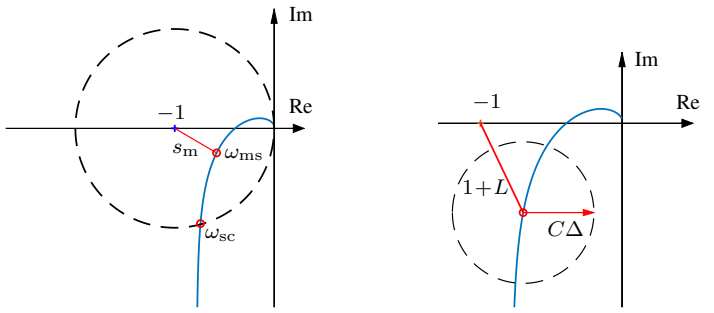

(a) Nyquist plot (b) Additive uncertainty

Figure 13.7: Illustrations of robust stability in Nyquist plots. The plot (a) shows the stability margin $s_m = 1/M_s$. The plot (b) shows the Nyquist curve and the circle shows uncertainty due to stable additive process variations Δ.

changed from P to $P+\Delta$, the loop transfer function changes from PC to $PC+C\Delta$, as illustrated in Figure 13.7b. The additive perturbation Δ must be a stable transfer function to satisfy the winding number condition in the Nyquist theorem. If we have a bound on the size of Δ (represented by the dashed circle in the figure), then the system remains stable as long as the perturbed loop transfer function $|1+(P+\Delta)C|$ never reaches the critical point -1, since the number of encirclements of -1 remains unchanged.

We will now compute an analytical bound on the allowable process disturbances. The distance from the critical point -1 to the loop transfer function $L = PC$ is $|1 + L|$. This means that the perturbed Nyquist curve will not reach the critical point -1 provided that $|C\Delta| < |1 + L|$, which is guaranteed if

$$|\Delta| < \left|\frac{1+PC}{C}\right| = \left|\frac{1+L}{C}\right| \qquad \text{or} \qquad |\delta| < \frac{1}{|T|}, \quad \text{where} \quad \delta := \left|\frac{\Delta}{P}\right|. \tag{13.9}$$

This condition must be valid for all points on the Nyquist curve, i.e, pointwise for all frequencies. The condition for robust stability can thus be written as

$$|\delta(i\omega)| = \left|\frac{\Delta(i\omega)}{P(i\omega)}\right| < \left|\frac{1+L(i\omega)}{L(i\omega)}\right| = \frac{1}{|T(i\omega)|} \qquad \text{for all } \omega \geq 0. \tag{13.10}$$

Notice that the condition is conservative in the sense that the critical perturbation is in the direction toward the critical point -1. Larger perturbations can be permitted in the other directions.

Robustness is normally defined as the margin to maintain stability. It is easy to modify the criterion and obtain a robustness condition that guarantees a specified stability margin (Exercise 13.8).

The condition in equation (13.10) allows us to reason about uncertainty without exact knowledge of the process perturbations. Namely, we can verify stability for *any* uncertainty Δ that satisfies the given bound. From an analysis perspective, this gives us a measure of the robustness for a given design. Conversely, if we require robustness of a given level, we can attempt to choose our controller C such that the desired level of robustness is available (by asking that T be small) in the appropriate frequency bands.

Equation (13.10) is one of the reasons why feedback systems work so well in practice. The mathematical models used to design control systems are often simplified, and the properties of a process may change during operation. Equation (13.10) implies that the closed loop system will at least be stable for substantial variations in the process dynamics.

It follows from equation (13.10) that the variations can be large for those frequencies where T is small and that smaller variations are allowed for frequencies where T is large. A conservative estimate of permissible process variations that will not cause instability is given by

$$|\delta(i\omega)| = \Big|\frac{\Delta(i\omega)}{P(i\omega)}\Big| < \frac{1}{|T(i\omega)|} \leq \frac{1}{M_{\mathrm{t}}}, \tag{13.11}$$

where M_{t} is the largest value of the complementary sensitivity

$$M_{\mathrm{t}} = \sup_{\omega} |T(i\omega)| = \Big\|\frac{PC}{1+PC}\Big\|_{\infty}. \tag{13.12}$$

Reasonable values of M_{t} are in the range of 1.2 to 2. It is shown in Exercise 13.9 that if $M_{\mathrm{t}} = 2$ then pure gain variations of 50% or pure phase variations of 30° are permitted without making the closed loop system unstable.

Example 13.7 Cruise control
Consider the cruise control system discussed in Section 4.1. Using the parameters from Example 6.11, the model of the car in fourth gear at speed 20 m/s is

$$P(s) = \frac{1.32}{s + 0.01},$$

and the controller is a PI controller with gains $k_{\mathrm{p}} = 0.5$ and $k_{\mathrm{i}} = 0.1$. Figure 13.8 plots the allowable size of the process uncertainty using the bound in equation (13.10).

At low frequencies, $T(0) = 1$ and so the perturbations can be as large as the original process ($|\delta| = |\Delta/P| < 1$). The complementary sensitivity has its maximum $M_{\mathrm{t}} = 1.17$ at $\omega_{\mathrm{mt}} = 0.26$, and hence this gives the lowest allowable process uncertainty, with $|\delta| < 0.86$ or $|\Delta| < 4.36$. Finally, at high frequencies, $T \to 0$ and hence the relative error can get very large. For example, at $\omega = 5$ rad/s we have $|T(i\omega)| = 0.264$, which means that the stability requirement is $|\delta| < 3.8$. The analysis clearly indicates that the system has good robustness and that the high-frequency properties of the transmission system are not important for the design of the cruise controller.

Another illustration of the robustness of the system is given in Figure 13.8b, which shows the Nyquist curve of the loop transfer function L along with the allowable perturbations. We see that the system can tolerate large amounts of uncertainty and still maintain stability of the closed loop. ∇

The situation illustrated in the previous example is typical of many processes: moderately small uncertainties are required only around the gain crossover frequencies, but large uncertainties can be permitted at higher and lower frequencies. A consequence of this is that a simple model that describes the process dynamics well around the crossover frequency is often sufficient for design. Systems with many resonant peaks are an exception to this rule because the process transfer function

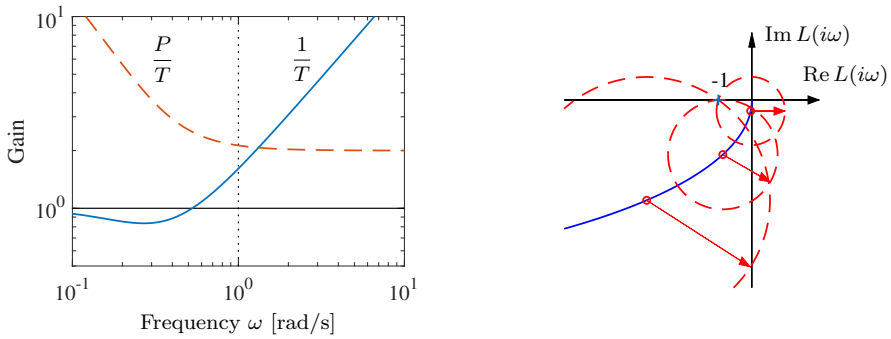

(a) Bounds on process uncertainty (b) Nyquist plot representation of bounds

Figure 13.8: Robustness for a cruise controller. (a) The maximum relative error $1/|T|$ (solid) and the absolute error $|P|/|T|$ (dashed) for the process uncertainty Δ. (b) The Nyquist plot of the loop transfer function L (zoomed in to the region around the critical point) is shown on the right as a solid line. The dashed circles show allowable perturbations in the process dynamics, $|C\Delta| = |CP|/|T|$, at the frequencies $\omega = 0.2$, 0.4, and 2, which are marked with circles.

for such systems may also have large gains for higher frequencies, as shown for instance in Example 10.9.

The robustness condition given by equation (13.10) can be given another interpretation by using the small gain theorem (Theorem 10.4). To apply the theorem we start with block diagrams of a closed loop system with a perturbed process and make a sequence of transformations of the block diagram that isolate the block representing the uncertainty, as shown in Figure 13.9. The result is the two-block interconnection shown in Figure 13.9c, which has the loop transfer function

$$L = \frac{PC}{1+PC}\,\frac{\Delta}{P} = T\delta.$$

Equation (13.10) implies that the largest loop gain is less than 1 and hence the system is stable via the small gain theorem.

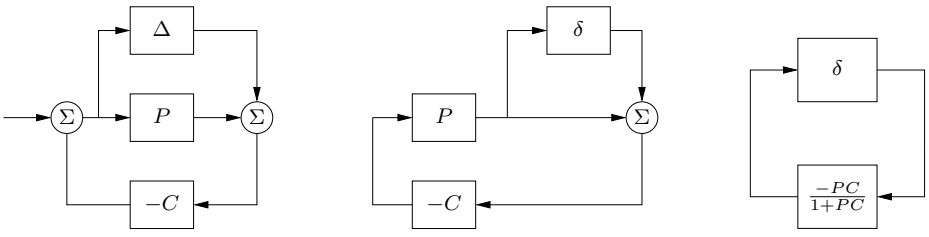

(a) Additive uncertainty (b) Multiplicative uncertainty (c) Small gain

Figure 13.9: Illustration of robustness to process perturbations. A system with additive uncertainty (a) can be manipulated via block diagram algebra to one with multiplicative uncertainty $\delta = \Delta/P$ (b). Additional manipulations isolate the uncertainty in a manner that allows application of the small gain theorem (c).

Table 13.1: Conditions for robust stability for different types of uncertainty

Process	Uncertainty Type	Robust Stability
$P + \Delta$	Additive	$\|CS\Delta\|_\infty < 1$
$P(1+\delta)$	Multiplicative	$\|T\delta\|_\infty < 1$
$P/(1+\Delta_{\text{fb}} \cdot P)$	Feedback	$\|PS\Delta_{\text{fb}}\|_\infty < 1$

The small gain theorem can be used to check robust stability for uncertainty in a variety of other situations. Table 13.1 summarizes a few of the common cases; the proofs (all via the small gain theorem) are left as exercises.

The circle criterion can also be used to understand robustness to nonlinear gain variations, as illustrated by the following example.

Example 13.8 Robustness for sector-bounded nonlinearities
Consider a system with a nonlinear gain $F(x)$ that can be isolated through appropriate manipulation of the block diagram, resulting in a system that is a feedback composition of the nonlinear block $F(x)$ and a linear part with the transfer function $H(s)$. If the nonlinearity is sector bounded,

$$k_{\text{low}}\, x < F(x) < k_{\text{high}}\, x,$$

and the nominal system has been designed to have maximum sensitivities M_{s} and M_{t}, we can use the circle criterion to verify stability of the closed loop system. In particular, the system can be shown to be stable for sector-bounded nonlinearities with

$$k_{\text{low}} = \frac{M_{\text{s}}}{M_{\text{s}}+1} \quad \text{or} \quad \frac{M_{\text{t}}-1}{M_{\text{t}}}, \qquad k_{\text{high}} = \frac{M_{\text{s}}}{M_{\text{s}}-1} \quad \text{or} \quad \frac{M_{\text{t}}+1}{M_{\text{t}}}.$$

With $M_{\text{s}} = M_{\text{t}} = 1.4$ we can thus permit gain variations from 0.3 to 3.5, and for a design with $M_{\text{s}} = M_{\text{t}} = 2$ we can allow gain variations of 0.5 to 2 without the system becoming unstable. ∇

The following example illustrates that it is possible to design systems that are robust to parameter variations.

Example 13.9 Bode's ideal loop transfer function
A major problem in the design of electronic amplifiers is to obtain a closed loop system that is insensitive to changes in the gain of the electronic components. Bode found that the loop transfer function

$$L(s) = ks^{-n}, \qquad 1 \le n \le 5/3 \tag{13.13}$$

had very useful robustness properties. The gain curve of the Bode plot is a straight line with slope $-n$ and the phase is constant $\arg L(i\omega) = -n\pi/2$. The phase margin is thus $\varphi_{\text{m}} = 90(2-n)^\circ$ for all values of the gain k and the stability margin is $s_{\text{m}} = \sin \pi(1 - n/2)$. Bode called the transfer function the "ideal cut-off characteristic" [Bod60, pp. 454–458]; we will call it *Bode's ideal loop transfer function* in honor of Bode. The transfer function cannot be realized with lumped physical com-

ponents unless n is an integer, but it can be approximated over a given frequency range with a proper rational function for any n (Exercise 13.11). An operational amplifier circuit that has the approximate transfer function $G(s) = k/(s+a)$ is a realization of Bode's ideal transfer function with $n = 1$, as described in Example 9.2. Designers of operational amplifiers go to great efforts to make the approximation valid over a wide frequency range. ∇

Youla Parameterization

Since stability is such an essential property, it is useful to characterize all controllers that stabilize a given process. Such a representation, which is called a *Youla parameterization*, is also very useful when solving design problems because it makes it possible to search over all stabilizing controllers without the need to test stability explicitly.

We will first derive Youla's parameterization for a stable process with a rational transfer function P. A system with a given complementary sensitivity function T can be obtained by feedforward control with the stable transfer function Q where $T = PQ$. Assume that we want to implement the transfer function T by feedback with the controller C. Since $T = PC/(1 + PC) = PQ$, the controller transfer function and its input-output relation are

$$C = \frac{Q}{1 - PQ}, \qquad u = Q(r - y + Py). \tag{13.14}$$

A straightforward calculation gives the transfer functions for the Gang of Four as

$$S = 1 - PQ, \qquad PS = P(1 - PQ), \qquad CS = Q, \qquad T = PQ.$$

These transfer functions are all stable if P and Q are stable and the controller given by equation (13.14) is thus stabilizing. Indeed, it can be shown that all stabilizing controllers are in the form given by equation (13.14) for some choice of Q.

The closed loop system with the controller (13.14) can be represented by the block diagram in Figure 13.10a. Notice that the signal z is always zero in steady state, because it is a subtraction of identical signals. Using block diagram algebra we find from the figure that the transfer function of the closed loop system is PQ. The fact that there are two blocks with transfer function P in parallel in the block diagram implies that there are modes, corresponding to the poles of P, that are not reachable and observable. These modes are stable because we assumed that P was stable. Architectures similar to Figure 13.10a appear in the Smith predictor and the internal model controller that will be discussed later in Section 15.4.

The scheme in Figure 13.10a cannot be used when the process is unstable but we can make a similar construct. Consider a closed loop system where the process is a rational transfer function $P = n_\mathrm{p}/d_\mathrm{p}$, where d_p and n_p are polynomials with no common factors. Assume that the controller $C = n_\mathrm{c}/d_\mathrm{c}$, where d_c and n_c are polynomials without common factors, stabilizes the system in the sense that all sensitivity functions are stable. By introducing stable polynomials f_p and f_c we obtain

$$P = \frac{n_\mathrm{p}}{d_\mathrm{p}} = \frac{N_\mathrm{p}}{D_\mathrm{p}}, \qquad C = \frac{n_\mathrm{c}}{d_\mathrm{c}} = \frac{N_\mathrm{c}}{D_\mathrm{c}}, \tag{13.15}$$

where $N_\mathrm{p} = d_\mathrm{p}/f_\mathrm{p}$, $D_\mathrm{p} = n_\mathrm{p}/f_\mathrm{p}$, $N_\mathrm{c} = n_\mathrm{c}/f_\mathrm{c}$, and $D_\mathrm{c} = d_\mathrm{c}/f_\mathrm{c}$ are rational functions

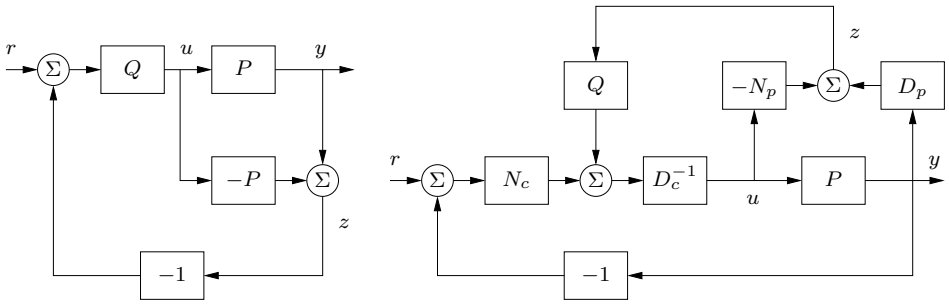

(a) Stable process (b) Unstable process

Figure 13.10: Block diagrams of Youla parameterizations for a stable process (a) and an unstable process (b). Notice that the signal z is zero in steady state in both cases.

with no zeros in the right half-plane (stable rational functions). The sensitivity functions are

$$S = \frac{1}{1+PC} = \frac{D_\mathrm{p}D_\mathrm{c}}{D_\mathrm{p}D_\mathrm{c}+N_\mathrm{p}N_\mathrm{c}}, \qquad PS = \frac{P}{1+PC} = \frac{N_\mathrm{p}D_\mathrm{c}}{D_\mathrm{p}D_\mathrm{c}+N_\mathrm{p}N_\mathrm{c}},$$
$$CS = \frac{C}{1+PC} = \frac{D_\mathrm{p}N_\mathrm{c}}{D_\mathrm{p}D_\mathrm{c}+N_\mathrm{p}N_\mathrm{c}}, \qquad T = \frac{PC}{1+PC} = \frac{N_\mathrm{p}N_\mathrm{c}}{D_\mathrm{p}D_\mathrm{c}+N_\mathrm{p}N_\mathrm{c}}.$$

The controller C is stabilizing if and only if the rational function $D_\mathrm{p}D_\mathrm{c}+N_\mathrm{p}N_\mathrm{c}$ does not have any zeros in the right half-plane. Letting Q be a stable rational function, we observe that the closed loop poles do not change if the controller C is changed by adding $N_\mathrm{p}Q$ to D_c and subtracting $D_\mathrm{p}Q$ from N_c, resulting in the controller

$$\bar{C} = \frac{N_\mathrm{c}-D_\mathrm{p}Q}{D_\mathrm{c}+N_\mathrm{p}Q}, \qquad D_\mathrm{c}u = N_\mathrm{c}(r-y)+Q(D_\mathrm{p}y-N_\mathrm{p}u)). \tag{13.16}$$

A block diagram of the closed loop system is shown in Figure 13.10b.

Figure 13.10b and 13.10a share the same basic structure, despite their difference in appearance. In both cases we form a signal z that is zero in steady state and feed it back into the system via the stable transfer function Q. The sensitivity functions of the closed loop system are

$$\begin{aligned} S &= \frac{1}{1+P\bar{C}} = \frac{D_\mathrm{p}(D_\mathrm{c}+N_\mathrm{p}Q)}{D_\mathrm{p}D_\mathrm{c}+N_\mathrm{p}N_\mathrm{c}}, & PS &= \frac{P}{1+P\bar{C}} = \frac{N_\mathrm{p}(D_\mathrm{c}+N_\mathrm{p}Q)}{D_\mathrm{p}D_\mathrm{c}+N_\mathrm{p}N_\mathrm{c}}, \\ \bar{C}S &= \frac{\bar{C}}{1+P\bar{C}} = \frac{D_\mathrm{p}(N_\mathrm{c}-D_\mathrm{p}Q)}{D_\mathrm{p}D_\mathrm{c}+N_\mathrm{p}N_\mathrm{c}}, & T &= \frac{P\bar{C}}{1+P\bar{C}} = \frac{N_\mathrm{p}(N_\mathrm{c}-D_\mathrm{p}Q)}{D_\mathrm{p}D_\mathrm{c}+N_\mathrm{p}N_\mathrm{c}}. \end{aligned} \tag{13.17}$$

These transfer functions are all stable and equation (13.16) is therefore a parameterization of controllers that stabilize the process P. Conversely it can be shown that all stabilizing controllers can be represented by the controller (13.16); see [Vid85, Section 3.1]. The controller $\bar{C}$ is a called a *Youla parameterization* of the controller C.

The Youla parameterization is very useful for controller design because it charac-

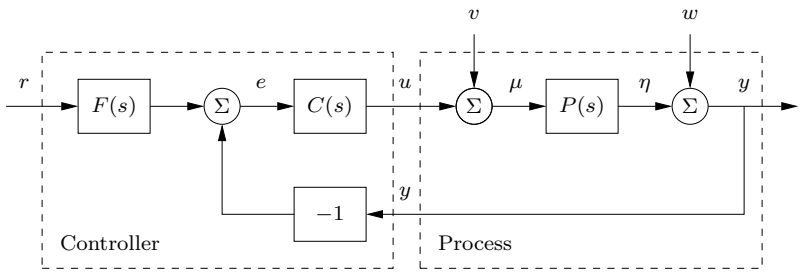

Figure 13.11: Block diagram of a basic feedback loop. The external signals are the reference signal r, the load disturbance v, and the measurement noise w. The process output is y, and the control signal is u. The process P may include unmodeled dynamics, such as additive perturbations.

terizes all controllers that stabilize a given process. The fact that the transfer function Q appears affinely in the expressions for the Gang of Four in equation (13.17) is very useful if we want to use optimization techniques to find a transfer function Q that yields desired closed loop properties.

13.3 PERFORMANCE IN THE PRESENCE OF UNCERTAINTY

So far we have investigated the risk for instability and robustness to process uncertainty. We will now explore how responses to load disturbances, measurement noise, and reference signals are influenced by process variations. To do this we will analyze the system in Figure 13.11, which is identical to the basic feedback loop analyzed in Chapter 12.

Disturbance Attenuation

The sensitivity function S gives a rough characterization of the effect of feedback on disturbances, as was discussed in Section 12.2. A more detailed characterization is given by the transfer function from load disturbances to process output:

$$G_{yv} = \frac{P}{1+PC} = PS. \tag{13.18}$$

Load disturbances typically have low frequencies, and it is therefore important that the transfer function G_{yv} is small for low frequencies. For processes P with constant low-frequency gain and a controller with integral action it follows from equation (13.18) that $G_{yv} \approx s/k_{\mathrm{i}}$. The integral gain k_{i} is thus a simple measure of the attenuation of low-frequency load disturbances.

To find out how the transfer function G_{yv} is influenced by small variations in the process transfer function we differentiate equation (13.18) with respect to P, yielding

$$\frac{dG_{yv}}{dP} = \frac{1}{(1+PC)^2} = \frac{SP}{P(1+PC)} = S\frac{G_{yv}}{P},$$

and it follows that

$$\frac{dG_{yv}}{G_{yv}} = S\frac{dP}{P}, \tag{13.19}$$

where we write dG and dP as a reminder that this expression holds for small variations.

In this form, we see that the relative error in the transfer function G_{yu} is determined by the relative error in the process transfer function, scaled by the sensitivity function S. The response to load disturbances is thus insensitive to process variations for frequencies where $|S(i\omega)|$ is small.

A drawback with feedback is that the controller feeds measurement noise into the system. It is thus also important that the control actions generated by measurement noise are not too large. It follows from Figure 13.11 that the transfer function G_{uw} from measurement noise to controller output is given by

$$G_{uw} = -\frac{C}{1+PC} = -\frac{T}{P}. \tag{13.20}$$

Since measurement noise typically has high frequencies, the transfer function G_{uw} should not be too large for high frequencies. The loop transfer function PC is typically small for high frequencies, which implies that $G_{uw} \approx C$ for large s. To avoid injecting too much measurement noise the high-frequency gain of the controller transfer function $C(s)$ should thus be small. This property is called *high-frequency roll-off*. Low-pass filtering of the measured signal is a simple way to achieve this property, and this is common practice in PID control; see Section 11.5.

To determine how the transfer function G_{uw} is influenced by small variations in the process transfer function, we differentiate equation (13.20):

$$\frac{dG_{uw}}{dP} = \frac{d}{dP}\left(-\frac{C}{1+PC}\right) = \frac{C}{(1+PC)^2}C = -T\frac{G_{uw}}{P}.$$

Rearranging the terms gives

$$\frac{dG_{uw}}{G_{uw}} = -T\frac{dP}{P}. \tag{13.21}$$

If PC is small for high frequencies the complementary sensitivity function is also small, and we find that process uncertainty has little influence on the transfer function G_{uw} for those frequencies.

Response to Reference Signals

The transfer function from reference to output is given by

$$G_{yr} = \frac{PCF}{1+PC} = TF, \tag{13.22}$$

which contains the complementary sensitivity function. To see how variations in P affect the performance of the system, we differentiate equation (13.22) with respect to the process transfer function:

$$\frac{dG_{yr}}{dP} = \frac{CF}{1+PC} - \frac{PCFC}{(1+PC)^2} = \frac{CF}{(1+PC)^2} = S\frac{G_{yr}}{P},$$

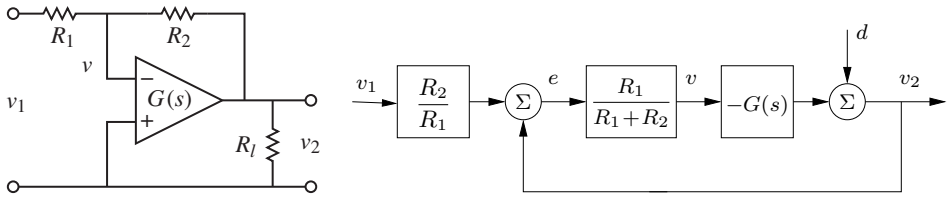

(a) Circuit diagram (b) Block diagram

Figure 13.12: Operational amplifier with uncertain dynamics. The circuit on the left is modeled using the transfer function $G(s)$ to capture its dynamic properties and it has a load at the output. The block diagram on the right shows the input/output relationships. The load is represented as a disturbance d applied at the output of $G(s)$.

and it follows that

$$\frac{dG_{yr}}{G_{yr}} = S\frac{dP}{P}. \tag{13.23}$$

The relative error in the closed loop transfer function thus equals the product of the sensitivity function and the relative error in the process. In particular, it follows from equation (13.23) that the relative error in the closed loop transfer function is small when the sensitivity is small. This is one of the useful properties of feedback.

As in the previous section, there are some mathematical assumptions that are required for the analysis presented here to hold. As already stated, we require that the perturbations Δ be small (as indicated by writing dP). Second, we require that the perturbations be stable, so that we do not introduce any new right half-plane poles that would require additional encirclements in the Nyquist criterion. Also, as before, this condition is conservative: it allows for any perturbation that satisfies the given bounds, while in practice the perturbations may be more restricted.

Example 13.10 Operational amplifier circuit
To illustrate the use of these tools, consider the performance of an op amp-based amplifier, as shown in Figure 13.12a. We wish to analyze the performance of the amplifier in the presence of uncertainty in the dynamic response of the op amp and changes in the loading on the output. We model the system using the block diagram in Figure 13.12b, which is based on the derivation in Exercise 10.1.

Consider first the effect of unknown dynamics for the operational amplifier. Letting the dynamics of the op amp be modeled as $v_2 = -G(s)v$, it follows from the block diagram in Figure 13.12b that the transfer function for the overall circuit is

$$G_{v_2v_1} = -\frac{R_2}{R_1}\frac{G(s)}{G(s) + R_2/R_1 + 1}.$$

We see that if $G(s)$ is large over the desired frequency range, then the closed loop system is very close to the ideal response $\alpha := R_2/R_1$. Assuming $G(s) = b/(s+a)$, where $b = ak$ is the gain-bandwidth product of the amplifier (as discussed in Example 9.2), the sensitivity function and the complementary sensitivity function become

$$S = \frac{s+a}{s+a+\alpha b}, \qquad T = \frac{\alpha b}{s+a+\alpha b}.$$

The sensitivity function around the nominal values tells us how the tracking re-

sponse varies as a function of process perturbations:

$$\frac{dG_{v_2v_1}}{G_{v_2v_1}} = S\frac{dP}{P}.$$

We see that for low frequencies, where S is small, variations in the bandwidth a or the gain-bandwidth product b will have relatively little effect on the performance of the amplifier (under the assumption that b is sufficiently large).

To model the effects of an unknown load, we consider the addition of a disturbance d at the output of the system, as shown in Figure 13.12b. This disturbance represents changes in the output voltage due to loading effects. The transfer function $G_{v_2d} = S$ gives the response of the output to the load disturbance, and we see that if S is small, then we are able to reject such disturbances. The sensitivity of G_{v_2d} to perturbations in the process dynamics can be computed by taking the derivative of G_{v_2d} with respect to P:

$$\frac{dG_{v_2d}}{dP} = \frac{-C}{(1+PC)^2} = -\frac{T}{P}G_{v_2d} \qquad \Longrightarrow \qquad \frac{dG_{v_2d}}{G_{v_2d}} = -T\frac{dP}{P}.$$

Thus we see that the relative changes in disturbance rejection are roughly the same as the process perturbations at low frequencies (when T is approximately 1) and drop off at higher frequencies. However, it is important to remember that G_{v_2d} itself is small at low frequency, and so these variations in relative performance may not be an issue in many applications. ∇

Analysis of the sensitivity to small process perturbations can performed for many other system configurations. The analysis for the system in Figure 12.13, where the reference signal response is improved by feedforward and the load disturbance response is improved by feedforward from measured disturbances, is presented in Exercise 13.6.

13.4 DESIGN FOR ROBUST PERFORMANCE

Control design is a rich problem where many factors have to be taken into account. Typical requirements are that load disturbances should be attenuated, the controller should inject only a moderate amount of measurement noise, the output should follow variations in the command signal well, and the closed loop system should be insensitive to process variations. For the system in Figure 13.11 these requirements can be captured by specifications on the sensitivity functions S and T and the transfer functions G_{yv}, G_{uw}, G_{yr}, and G_{ur}. Notice that it is necessary to consider at least six transfer functions, as discussed Section 12.1. The requirements are mutually conflicting, and we have to make trade-offs. The attenuation of load disturbances will be improved if the bandwidth is increased, but the noise injection will be worse. The following example is an illustration.

Example 13.11 Nanopositioning system for an atomic force microscope
A simple nanopositioner with the process transfer function

$$P(s) = \frac{\omega_0^2}{s^2 + 2\zeta\omega_0 s + \omega_0^2}$$

was explored in Example 10.9. It was shown that the system could be controlled using an integral controller. The closed-loop performance was poor because the gain crossover frequency was limited to $\omega_{gc} < 2\zeta\omega_0(1-s_m)$ to have good robustness with the integral controller. It can be shown that little improvement is obtained by using a PI controller. We will explore if better performance can be obtained with PID control. As justified in Example 14.11 in the next chapter, we trying choosing a controller zero that is near the fast stable process pole. The controller transfer function should thus be chosen as

$$C(s) = \frac{k_d s^2 + k_p s + k_i}{s} = \frac{k_i}{s}\frac{s^2 + 2\zeta\omega_0 s + \omega_0^2}{\omega_0^2}, \tag{13.24}$$

which gives $k_p = 2\zeta k_i/\omega_0$ and $k_d = k_i/\omega_0^2$. The loop transfer function becomes $L(s) = k_i/s$.

Figure 13.13 shows, in dashed lines, the gain curves for the Gang of Four for a system designed with $k_i = 0.5$. A comparison with Figure 10.14 shows that the bandwidth is increased significantly from $\omega_{gc} = 0.01$ to $\omega_{gc} = k_i = 0.5$. However, since the process pole is canceled, the system will be very sensitive to load disturbances with frequencies close to the resonant frequency, as seen by the peak in PS at $\omega/\omega_0 = 1$. The gain curve of CS has a dip or a notch at the resonant frequency ω_0, which implies that the controller gain is very low for frequencies around the resonance. The gain curve also shows that the system is very sensitive to high-frequency noise. The system will likely be unusable because the gain goes to infinity for high frequencies.

The sensitivity to high-frequency noise can be reduced by modifying the controller to be

$$C(s) = \frac{k_i}{s}\frac{s^2 + 2\zeta\omega_0 s + \omega_0^2}{\omega_0^2(1 + sT_f + (sT_f)^2/2)}, \tag{13.25}$$

which has high-frequency roll-off. Selection of the constant T_f for the filter is a compromise between attenuation of high-frequency measurement noise and robustness. A large value of T_f reduces the effects of sensor noise significantly, but it also reduces the stability margin. Since the gain crossover frequency without filtering is k_i, a reasonable choice is $T_f = 0.2/k_i$, as shown by the solid curves in Figure 13.13. The plots of $|CS(i\omega)|$ and $|S(i\omega)|$ show that the sensitivity to high-frequency measurement noise is reduced dramatically at the cost of a marginal increase of sensitivity. Notice that the poor attenuation of disturbances with frequencies close to the resonance is not visible in the sensitivity function because of the cancellation of the resonant poles (but it can be seen in PS).

The designs thus far have the drawback that load disturbances with frequencies close to the resonance are not attenuated, since $|S(i\omega_0)|$ is close to one. We will now consider a design that actively attenuates the poorly damped modes. We start with an ideal PID controller where the design can be done analytically, and we add high-frequency roll-off. The loop transfer function obtained with this controller is

$$L(s) = \frac{\omega_0^2(k_d s^2 + k_p s + k_i)}{s(s^2 + 2\zeta\omega_0 s + \omega_0^2)}. \tag{13.26}$$

The closed loop system is of third order, and its characteristic polynomial is

$$s^3 + (k_d\omega_0^2 + 2\zeta\omega_0)s^2 + (k_p + 1)\omega_0^2 s + k_i\omega_0^2. \tag{13.27}$$

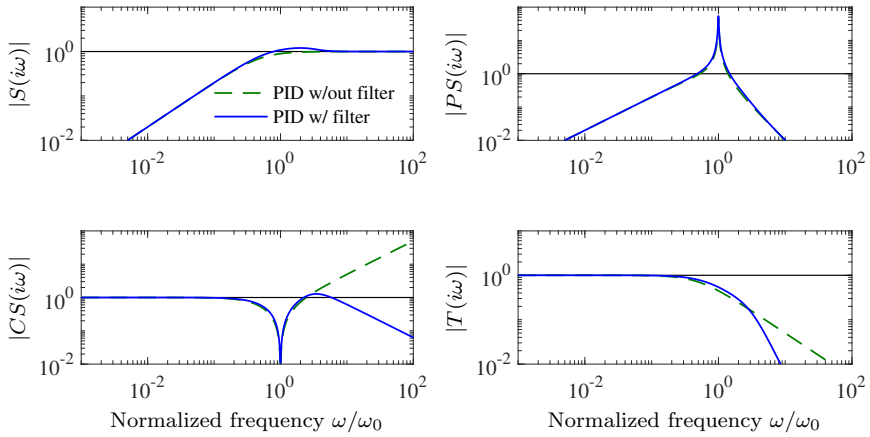

Figure 13.13: Nanopositioning system control via cancellation of the fast process pole. Gain curves for the Gang of Four for PID control with second-order filtering (13.25) are shown by solid lines, and the dashed lines show results for an PID controller without filtering (13.24).

A general third-order polynomial can be parameterized as

$$s^3 + (\alpha_c + 2\zeta_c)\omega_c s^2 + (1 + 2\alpha_c\zeta_c)\omega_c^2 s + \alpha_c\omega_c^3. \tag{13.28}$$

The parameters α_c and ζ_c give the relative configuration of the poles, and the parameter ω_c gives their magnitudes, and therefore also the bandwidth of the system.

The identification of coefficients of equal powers of s with equation (13.27) gives a linear equation for the controller parameters, which has the solution

$$k_p = \frac{(1 + 2\alpha_c\zeta_c)\omega_c^2}{\omega_0^2} - 1, \qquad k_i = \frac{\alpha_c\omega_c^3}{\omega_0^2}, \qquad k_d = \frac{(\alpha_c + 2\zeta_c)\omega_c}{\omega_0^2} - \frac{2\zeta_c}{\omega_0}. \tag{13.29}$$

Adding high-frequency roll-off, the controller becomes

$$C(s) = \frac{k_d s^2 + k_p s + k}{s(1 + sT_f + (sT_f)^2/2)}. \tag{13.30}$$

If the PID controller is designed without the filter, the filter time constant must be significantly smaller than T_d to avoid introducing extra phase lag; a reasonable value is $T_f = T_d/10 = 0.1\, k_d/k$. If more filtering is desired it is necessary to account for the filter dynamics in the design.

Figure 13.14 shows the gain curves of the Gang of Four for designs with $\zeta_c = 0.707$, $\alpha_c = 1$, and $\omega_c = \omega_0$, $2\omega_0$, and $4\omega_0$. The figure shows that the largest values of the sensitivity functions S and T are small. The gain curve for PS shows that the load disturbances are now well attenuated over the whole frequency range, and attenuation increases with increasing ω_0. The gain curve for CS shows that large control signals are required to provide active damping. The high gain of CS for high frequencies also shows that low-noise sensors and actuators with a wide range are required. The largest gains for CS are 19, 103 and 434 for $\omega_c = \omega_0$, $2\omega_0$, and $4\omega_0$, respectively. There is clearly a trade-off between disturbance attenuation and controller gain. A comparison of Figures 13.13 and 13.14 illustrates the trade-offs

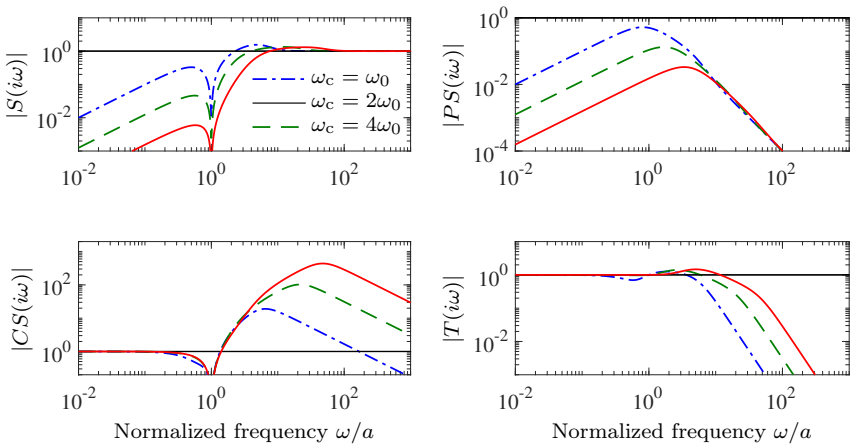

Figure 13.14: Nanopositioner control using active damping. Gain curves for the Gang of Four for PID control of the nanopositioner designed for $\omega_c = \omega_0$ (dash-dotted), $2\omega_0$ (dashed), and $4\omega_0$ (solid). The controller has high-frequency roll-off and has been designed to give active damping of the oscillatory mode. The different curves correspond to different choices of magnitudes of the poles, parameterized by ω_c in equation (13.27).

between control action and disturbance attenuation for the designs with cancellation of the fast process pole and active damping. ∇

It is highly desirable to have design methods that can guarantee robust performance. Such design methods did not appear until the late 1980s. Many of these design methods result in controllers having the same structure as the controller based on state feedback and an observer. In remainder of this section we provide a brief review of some of the techniques as a preview for those interested in more specialized study.

Quantitative Feedback Theory

Quantitative feedback theory (QFT) is a graphical design method for robust loop shaping that was developed by I. M. Horowitz [Hor91]. The idea is to first determine a controller that gives a complementary sensitivity that is robust to process variations and then to shape the response to reference signals by feedforward. The idea is illustrated in Figure 13.15a, which shows the level curves of the gain $|T(i\omega)|$ of the complementary sensitivity function on a Nyquist plot (this type of Nyquist plot is also called a *Hill chart*). The complementary sensitivity function has unit gain on the line $\operatorname{Re} L(i\omega) = -0.5$. In the neighborhood of this line, significant variations in process dynamics only give moderate changes in the complementary transfer function. The shaded part of the figure corresponds to the region $0.9 < |T(i\omega)| < 1.1$. To use the design method, we represent the uncertainty for each frequency by a region and attempt to shape the loop transfer function so that the variation in T is as small as possible. The design is often performed using the Nichols chart shown in Figure 13.15b.

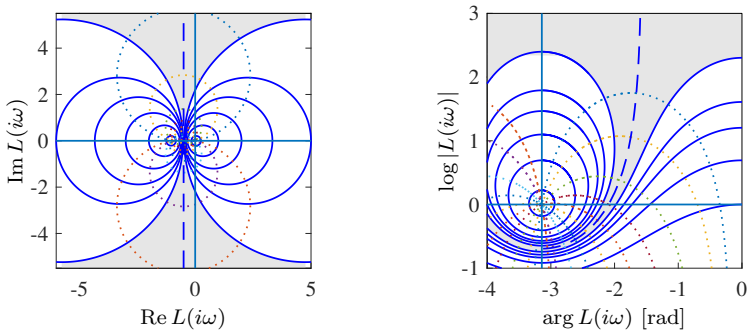

(a) Hall chart (b) Nichols chart

Figure 13.15: Hall and Nichols charts. The Hall chart is a Nyquist plot with curves for constant gain (solid) and phase (dotted) of the complementary sensitivity function T. The Nichols chart is the conformal map of the Hall chart under the transformation $N = \log L$ (with the scale flipped). The dashed curve is the line where $|T(i\omega)| = 1$, and the shaded region corresponds to loop transfer functions whose complementary sensitivity changes by no more than $\pm 10\%$.

Linear Quadratic Control

One way to make the trade-off between the attenuation of load disturbances and the injection of measurement noise is to design a controller that minimizes the cost function

$$J = \int_0^\infty \left(y^2(t) + \rho u^2(t)\right) dt,$$

where ρ is a weighting parameter as discussed in Section 8.4. This cost function gives a compromise between load disturbance attenuation and disturbance injection because it balances control actions against deviations in the output. If all state variables are measured, the controller is a state feedback $u = -Kx$ as described in Section 7.5. It has been shown that this controller is very robust: it has a phase margin of at least 60° and an infinite gain margin. This controller is called a *linear quadratic regulator* or *LQR controller* because the process model is linear and the criterion is quadratic.

When all state variables are not measured, the state can be reconstructed using an observer, as discussed in Section 8.3. It is also possible to introduce process disturbances and measurement noise explicitly in the model and to reconstruct the states using a Kalman filter, as discussed briefly in Section 8.4. The Kalman filter has the same structure as the observer designed by eigenvalue assignment in Section 8.3, but the observer gains L are now obtained by solving an optimization problem.

The control law obtained by combining linear quadratic control with a Kalman filter is called *linear quadratic Gaussian control* or *LQG control*. The Kalman filter is optimal when the models for load disturbances and measurement noise are Gaussian. There are efficient programs to compute these feedback and observer gains. The basic task is to solve algebraic Riccati equations. For numerical calculations we can use the MATLAB commands `care` for continuous time systems and `dare` for discrete time systems. The are also MATLAB commands `lqg`, `lqi`, and `kalman` that perform the complete design.

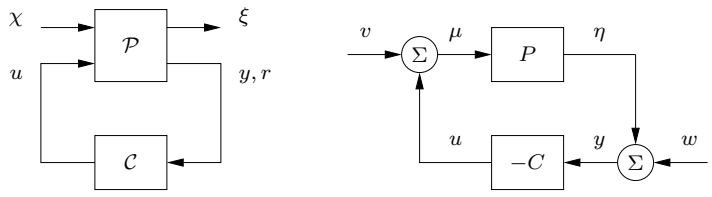

(a) General structure (b) Special structure

Figure 13.16: H_∞ robust control formulation. (a) General representation of a control problem used in robust control. The input u represents the control signal, the input χ represents the external influences on the system, the output ξ is the generalized error and the output y is the measured signal. (b) Special case of the basic feedback loop in Figure 13.11 where the reference signal is zero.

It is interesting that the solution to the optimization problem leads to a controller having the structure of a state feedback and an observer. The state feedback gains depend on the parameter ρ, and the filter gains depend on the parameters in the model that characterize process noise and measurement noise (see Section 8.4).

The nice robustness properties of state feedback are unfortunately lost when the observer is added [Doy78]. There are parameters that give closed loop systems with poor robustness, and hence there is a fundamental difference between directly measuring the states of a system and reconstructing the states using an observer.

H_∞ Control

An elegant method for robust control design is called H_∞ control because it can be formulated as minimization of the H_∞ norm of a matrix of transfer functions, defined in equation (10.15). The basic ideas are simple, but the details are complicated and we will therefore just give the flavor of the results. A key idea is illustrated in Figure 13.16a, where the closed loop system is represented by two blocks the process $\mathcal{P}$ and the controller $\mathcal{C}$ as discussed in Section 12.1. The process $\mathcal{P}$ has two inputs, the control signal u, which can be manipulated by the controller, and the generalized disturbance χ, which represents all external influences, e.g., command signals, load disturbances, and measurement noise. The process has two outputs, the generalized error ξ, which is a vector of error signals representing the deviation of signals from their desired values, and the measured signal y, which can be used by the controller to compute u. For a linear system and a linear controller the closed loop system can be represented by the linear system

$$\xi = \mathcal{G}(P(s), C(s))\chi, \tag{13.31}$$

which tells how the generalized error ξ depends on the generalized disturbances χ. The control design problem is to find a controller C such that the gain of the transfer function $\mathcal{G}$ is small even when the process has uncertainties. There are many different ways to specify uncertainty and gain, giving rise to different designs depending on the chosen norms.

To illustrate the ideas we will consider a regulation problem for a system where the reference signal is assumed to be zero and the external signals are the load disturbance v and the measurement noise w, as shown in Figure 13.16b. The generalized error is defined as $\xi = (\mu, \eta)$, where $\mu = v - u$ is the part of the load

disturbance that is not compensated by the controller and η is the process output. The generalized input is $\chi = (v, -w)$ (the negative sign of w is not essential but is chosen to obtain somewhat nicer equations). The closed loop system is thus modeled by

$$\xi = \begin{pmatrix} \mu \\ \eta \end{pmatrix} = \begin{pmatrix} \dfrac{1}{1+PC} & \dfrac{C}{1+PC} \\ \dfrac{P}{1+PC} & \dfrac{PC}{1+PC} \end{pmatrix} \begin{pmatrix} v \\ -w \end{pmatrix} = \mathcal{G}(P,C)\chi, \tag{13.32}$$

which is a special case of equation (13.31). If C is stabilizing we have

$$\|\mathcal{G}(P,C))\|_\infty = \sup_\omega \bar{\sigma}(\mathcal{G}) = \sup_\omega \frac{\sqrt{(1+|P(i\omega)|^2)(1+|C(i\omega)|^2)}}{|1+P(i\omega)C(i\omega)|}. \tag{13.33}$$

where $\bar{\sigma}$ is the largest singular value. Notice that the elements of $\mathcal{G}$ are the Gang of Four. The diagonal elements of $\mathcal{G}$ are the sensitivity functions $S = 1/(1+PC)$ and $T = PC/(1+PC)$, which capture robustness. The off-diagonal elements $P/(1+PC) = G_{yv}$ and $C/(1+PC) = -G_{uw}$ represent the the responses of the output to load disturbances and of the control signal to measurement noise, and they capture performance. If we minimize $\|\mathcal{G}(P,C)\|_\infty$, we thus balance performance and robustness.

There are numerical methods for finding a stabilizing controller C that minimizes $\|\mathcal{G}(P,C)\|_\infty$, if such a controller exists. This controller has the same structure as the controller based on state feedback and an observer; see Figure 8.7 and Theorem 8.3. The controller gains are given by *algebraic Riccati* equations. They can be computed numerically by the MATLAB command `hinfsyn`.

The Generalized Stability Margin

In Section 13.2 we introduced the stability margin as $s_{\mathrm{m}} = \inf_\omega |1 + P(i\omega)C(i\omega)|$ for systems such that C stabilizes P. The margin can be interpreted as the shortest distance between the Nyquist plot of the loop transfer function PC and the critical point -1, as shown in Figure 13.7a. We can also found that $s_{\mathrm{m}} = 1/M_{\mathrm{s}}$ where M_{s} is the maximum sensitivity. We now define the *generalized stability margin*

$$\sigma_{\mathrm{m}} = \begin{cases} \inf_\omega \dfrac{|1+P(i\omega)C(i\omega)|}{\sqrt{(1+|P(i\omega)|^2)(1+|C(i\omega)|^2)}} & \text{if } C \text{ stabilizes } P, \\ 0 & \text{otherwise.} \end{cases} \tag{13.34}$$

Since

$$\inf_\omega \frac{|1+P(i\omega)C(i\omega)|}{\sqrt{(1+|P(i\omega)|^2)(1+|C(i\omega)|^2)}} = \inf_\omega \frac{|P(i\omega)+1/C(i\omega)|}{\sqrt{(1+|P(i\omega)|^2)(1+|1/C(i\omega)|^2)}},$$

it follows that σ_{m} can be interpreted as the shortest chordal distance between $P(i\omega)$ and $-1/C(i\omega)$. Furthermore equations (13.6) and (13.33) imply that

$$\sigma_{\mathrm{m}}(P,C) = \begin{cases} \dfrac{1}{\|\mathcal{G}(P,C)\|_\infty} & \text{if } C \text{ stabilizes } P, \\ 0 & \text{otherwise.} \end{cases} \tag{13.35}$$

Using the generalized stability margin we have the following fundamental robustness theorem, which is proved in [Vin01].

Theorem 13.1 (Vinnicombe's robustness theorem)**.** *Consider a process with transfer function P. Assume that the controller C is designed to give the generalized stability margin σ_{m}. Then the controller C will stabilize all processes P_1 such that $\delta_\nu(P, P_1) < \sigma_{\mathrm{m}}(P, C)$, where δ_ν is the Vinnicombe metric.*

The theorem is a generalization of equation (13.11). The generalized stability margins can be related to the classical gain and phase margins. It follows from equation (13.34) that

$$|1 + P(i\omega)C(i\omega)|^2 \geq \sigma_{\mathrm{m}}^2(1 + |P(i\omega)|^2)(1 + |C(i\omega)|^2). \tag{13.36}$$

If the Nyquist curve of the loop transfer function PC intersects the negative real axis for some ω we have $P(i\omega)C(i\omega) = -k$ for some $0 < k < 1$ and equation (13.36) becomes

$$|1 - k|^2 \geq \sigma_{\mathrm{m}}^2(1 + |P(i\omega)|^2 + |C(i\omega)|^2 + k^2) \geq \sigma_{\mathrm{m}}^2(1 + k)^2,$$

which implies that

$$k \leq \frac{1 - \sigma_{\mathrm{m}}}{1 + \sigma_{\mathrm{m}}}, \qquad g_{\mathrm{m}} = \frac{1}{k} \geq \frac{1 + \sigma_{\mathrm{m}}}{1 - \sigma_{\mathrm{m}}}. \tag{13.37}$$

If the loop transfer function intersects the unit circle so that the phase margin is φ_{m} we have $P(i\omega)C(i\omega) = e^{i(\pi+\varphi_{\mathrm{m}})} = -e^{i\varphi_{\mathrm{m}}}$ and equation (13.36) becomes

$$|1 - e^{i\varphi_{\mathrm{m}}}|^2 \geq \sigma_{\mathrm{m}}^2(1 + |P(i\omega)|^2 + 1/|P(i\omega)|^2 + 1) \geq 4\sigma_{\mathrm{m}}^2,$$

where the last inequality follows from the fact that $|x|+1/|x| \geq 2$. Since $|1-e^{i\varphi_{\mathrm{m}}}| = 2\sin(\varphi_{\mathrm{m}}/2)$ (think geometrically) it follows that the above inequality can be written as

$$4\sin(\varphi_{\mathrm{m}}/2) \geq 4\sigma_{\mathrm{m}}^2, \qquad \varphi_{\mathrm{m}} \geq 2\arcsin\sigma_{\mathrm{m}} \tag{13.38}$$

(compare with equation 10.7). For $\sigma_{\mathrm{m}} = 1/3,\ 1/2,\ 2/3$ we have $g_{\mathrm{m}} \geq 2,\ 3,\ 5$ and $\varphi_{\mathrm{m}} \geq 39°,\ 60°,\ 84°$.

Disturbance Weighting

H_∞ control attempts to find a controller that minimizes the effect of external signals (χ in Figure 13.16a or ν and w in Figure 13.16b) on the generalized error ξ, in the sense that the largest singular value of the matrix $\|\mathcal{G}(P, C)\|_\infty$ is as small as possible. The solution of the problem can be changed by introducing weights W, which is illustrated in Figure 13.17a.

Figures 13.17b and 13.17c show how the problem with a weight W can be transformed into a problem of the same form as in Figure 13.17a. This allows the weighted problem to be solved using the same tools as the unweighted problem. In the transformed problem the process transfer function P is replaced by $\overline{P} = PW$ and the controller transfer function is replaced by $\overline{C} = W^{-1}C$. The relation between

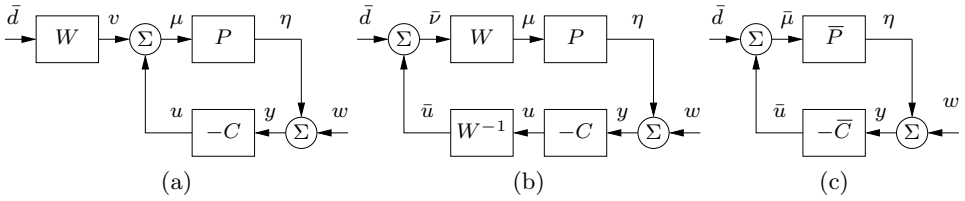

Figure 13.17: Block diagrams that illustrate frequency weighting of load disturbances. A frequency weight W is introduced on the load disturbance in (a). Block diagram transformations are used in (b) to obtain a system in standard form, which is redrawn in (c) using $\overline{P} = PW$ and $\overline{C} = W^{-1}C$.

the transformed signals then becomes

$$\bar{\xi} = \begin{pmatrix} \bar{\mu} \\ \bar{\eta} \end{pmatrix} \begin{pmatrix} \dfrac{1}{1 + \overline{P}\,\overline{C}} & \dfrac{\overline{P}}{1 + \overline{P}\,\overline{C}} \\ \dfrac{\overline{C}}{1 + \overline{P}\,\overline{C}} & \dfrac{\overline{P}\,\overline{C}}{1 + \overline{P}\,\overline{C}} \end{pmatrix} \begin{pmatrix} \bar{v} \\ -w \end{pmatrix} = \mathcal{G}(\overline{P}, \overline{C})\bar{\chi},$$

where $\overline{P} = PW$ and $\overline{C} = W^{-1}C$. Notice that $\overline{P}\overline{C} = PC$, which means that only the off diagonal block elements in the matrix $\mathcal{G}(\overline{P}, \overline{C})$ are different from those in $\mathcal{G}(P, C)$. Weighting thus does not change the sensitivity and complementary sensitivity functions. The matrix element corresponding to load disturbances changes from $P/(1 + PC)$ to $PW/(1 + PC)$ and the matrix element corresponding to measurement noise changes from $C/(1 + PC)$ to $CW^{-1}/(1 + PC)$.

Having chosen the desired weight W, the solution to the weighted H_∞ problem gives the controller $\overline{C}$. Transforming back then gives the real controller $C = W\overline{C}$. Choosing proper weights allows the designer to obtain a controller that reflects the design specifications. If W is a scalar greater than one it means that we are increasing the effect of the load disturbances and reducing the effect of the measurement noise. The weighting can also be made frequency dependent. For example, choosing the weight as $W = k/s$ will automatically give a controller with integral action. Similarly a weighting that emphasizes high frequencies will give a controller with high-frequency roll-off. Frequency weighting allows the designer to modify the solution to reflect the many different design specifications, making H_∞ loop shaping a very powerful design method.

Limits of Robust Design

There is a limit to what can be achieved by robust design. In spite of the nice properties of feedback, there are situations where the process variations are so large that it is not possible to find a linear controller that gives a robust system with good performance. It is then necessary to use other types of controllers. In some cases it is possible to measure a variable that is well correlated with the process variations. Controllers for different parameter values can then be designed and the corresponding controller can be chosen based on the measured signal. This type of control design is called *gain scheduling* and it was discussed briefly already in Section 8.5. The cruise controller is a typical example where the measured signal

could be gear position and velocity. Gain scheduling is the common solution for high-performance aircraft where scheduling is done based on Mach number and dynamic pressure. When using gain scheduling, it is important to make sure that switches between the controllers do not create undesirable transients (often referred to as the *bumpless transfer* problem).

It is often not possible to measure variables related to the parameters, in which case *automatic tuning* and *adaptive control* can be used. In automatic tuning the process dynamics are measured by perturbing the system, and a controller is then designed automatically. Automatic tuning requires that parameters remain constant, and it has been widely applied for PID control. It is a reasonable guess that in the future many controllers will have features for automatic tuning. If parameters are changing, it is possible to use adaptive methods where process dynamics are measured online.

13.5 FURTHER READING

The topic of robust control is a large one, with many articles and textbooks devoted to the subject. Robustness was a central issue in classical control as described in the books by Bode [Bod45], James, Nichols, and Phillips [JNP47], and Horowitz [Hor63]. Quantitative feedback theory (QFT) [Hor93] can be regarded as an extension of Bode's work. The interesting properties of Bode's ideal loop transfer function were rediscovered in the late 1990s, creating an interest in fractional transfer functions [MCM+10]. It took a long time before the fundamental question of when two systems are similar was clearly formulated. The gap metric was introduced by Zames and El-Sakkary [ZES80], and Vidyasagar introduced the graph metric a few year later [Vid84, Vid85]. The ν-gap metric, which is the proper notion, is due to Vinnicombe [Vin93, Vin01]. Robustness was deemphasized in the euphoria of the development of design methods based on optimization. The strong robustness of controllers based on state feedback, shown by Anderson and Moore [AM90], contributed to the optimism. The poor robustness of output feedback was pointed out by Rosenbrock [RM71], Horowitz [Hor75], and Doyle [Doy78] and resulted in a renewed interest in robustness. A major step forward was the development of design methods where robustness was explicitly taken into account, such as the seminal work of Zames [Zam81]. Robust control was originally developed using powerful results from the theory of complex variables, which gave controllers of high order. A major breakthrough was made by Doyle, Glover, Khargonekar, and Francis [DGKF89], who showed that the solution to the problem could be obtained using Riccati equations and that a controller of low order could be found. This paper led to an extensive treatment of H_∞ control, including books by Francis [Fra87], McFarlane and Glover [MG90], Doyle, Francis, and Tannenbaum [DFT92], Green and Limebeer [GL95], Zhou, Doyle, and Glover [ZDG96], Skogestad and Postlethwaite [SP05], and Vinnicombe [Vin01]. A major advantage of the theory is that it combines much of the intuition from servomechanism theory with sound numerical algorithms based on numerical linear algebra and optimization. The results have been extended to nonlinear systems by treating the design problem as a game where the disturbances are generated by an adversary, as described in the book by Basar and Bernhard [BB91]. Gain scheduling and adaptation are discussed in the book by Åström and Wittenmark [ÅW08a].

EXERCISES

13.1 Consider systems with the transfer functions $P_1 = 1/(s+1)$ and $P_2 = 1/(s+a)$. Show that P_1 can be changed continuously to P_2 with bounded additive and multiplicative uncertainty if $a > 0$ but not if $a < 0$. Also show that no restriction on a is required for feedback uncertainty.

13.2 Consider systems with the transfer functions $P_1 = (s+1)/(s+1)^2$ and $P_2 = (s+a)/(s+1)^2$. Show that P_1 can be changed continuously to P_2 with bounded feedback uncertainty if $a > 0$ but not if $a < 0$. Also show that no restriction on a is required for additive and multiplicative uncertainties.

13.3 (Difference in sensitivity functions) Let $T(P, C)$ be the complementary sensitivity function for a system with process P and controller C. Show that

$$T(P_1, C) - T(P_2, C) = \frac{(P_1 - P_2)C}{(1 + P_1C)(1 + P_2C)},$$

and compare with equation (13.6). Derive a similar formula for the sensitivity function.

13.4 (Diametrically opposite points) Consider the points $z = a$ and $z = -1/a$ in the complex plane. Show that their projections on the Riemann sphere are diametrically opposite and hence their chordal distance is 1.

13.5 (Vinnicombe metrics) Consider the transfer functions

$$P_1(s) = \frac{k}{4s+1}, \qquad P_2(s) = \frac{k}{(2s+1)^2}, \qquad P_3(s) = \frac{k}{(s+1)^4}$$

Compute the Vinnicombe metric for all combinations of the transfer functions when $k = 1$ and $k = 2$. Discuss the results.

13.6 (Sensitivity of two degree-of-freedom controllers to process variations) Consider the two degree-of-freedom controller shown in Figure 12.13, which uses feedforward compensation to provide improved response to reference signals and measured disturbances. Show that the input/output transfer functions and the corresponding sensitivities to process variations for the feedforward, feedback, and combined controllers are given by

Controller	G_{yr}	$\frac{dG_{yr}}{G_{yr}}$	G_{yv}	$\frac{dG_{yv}}{dP_1}$
Feedforward ($C = 0$)	F_{m}	$\frac{dP}{P}$	0	$-\frac{P_2}{P_1}$
Feedback (F_r, $F_v = 0$)	TF_{m}	$S\,\frac{dP}{P}$	$S\,P_2$	$-S\,\frac{P_2}{P_1}$
Feedforward and Feedback	F_{m}	$S\,\frac{dP}{P}$	0	$S\,\frac{P_2}{P_1}$

13.7 (Sensitivity of feedback and feedforward) Consider the system in Figure 13.11 and let G_{yr} be the transfer function relating the measured signal y to the reference r. Show that the sensitivities of G_{yr} with respect to the feedforward and feedback

transfer functions F and C are given by $dG_{yr}/dF = CP/(1+PC)$ and $dG_{yr}/dC = FP/(1+PC)^2 = G_{yr}S/C$.

13.8 (Guaranteed stability margin) The inequality given by equation (13.10) guarantees that the closed loop system is stable for process uncertainties. Let $s_{\mathrm{m}}^0 = 1/M_{\mathrm{s}}^0$ be a specified stability margin. Show that the inequality

$$|\delta(i\omega)| < \frac{1 - s_{\mathrm{m}}^0 |S(i\omega)|}{|T(i\omega)|} = \frac{1 - |S(i\omega)|/M_{\mathrm{s}}^0}{|T(i\omega)|}, \qquad \text{for all } \omega \geq 0,$$

guarantees that the closed loop system has a stability margin greater than s_{m}^0 for all perturbations (compare with equation (13.10)).

13.9 (Stability margins) Consider a feedback loop with a process and a controller having transfer functions P and C. Assume that the maximum sensitivity is $M_{\mathrm{s}} = 2$. Show that the phase margin is at least 30° and that the closed loop system will be stable if the gain is changed by 50%.

13.10 (Bode's ideal loop transfer function) Bode's ideal loop transfer function is given in Example 13.9. Show that the phase margin is φ_{m} =180°–90°n and that the stability margin is $s_{\mathrm{m}} = \sin \pi(1 - n/2)$. Make Bode and Nyquist plots of the transfer function for n=5/3.

13.11 Consider a process with the transfer function $P(s) = k/(s(s+1))$, where the gain can vary between 0.1 and 10. A controller that has a phase margin close to $\varphi_{\mathrm{m}} = 45°$ for the gain variations can be obtained by finding a controller that gives the loop transfer function $L(s) = 1/(s\sqrt{s})$. Suggest how the transfer function can be implemented by approximating it by a rational function.

13.12 (Smith predictor) The *Smith predictor*,, a controller for systems with time delays, is a special version of Figure 13.10a with $P(s) = e^{-s\tau}P_0(s)$ and $Q(s) = C_0(s)/(1 + C_0(s)P(s))$. The controller $C_0(s)$ is designed to give good performance for the process $P_0(s)$. Show that the sensitivity functions are

$$S(s) = \frac{1 + (1 - e^{-s\tau})P_0(s)C_0(s)}{1 + P_0(s)C_0(s)}, \qquad T(s) = \frac{P_0(s)C_0(s)}{1 + P_0(s)C_0(s)} e^{-s\tau}.$$

13.13 (Ideal delay compensator) Consider a process whose dynamics are a pure time delay with transfer function $P(s) = e^{-s}$. The ideal delay compensator is a controller with the transfer function $C(s) = 1/(1 - e^{-s})$. Show that the sensitivity functions are $T(s) = e^{-s}$ and $S(s) = 1 - e^{-s}$ and that the closed loop system will be unstable for arbitrarily small changes in the delay.

13.14 (Pole/zero cancellation) Consider the system in Figure 13.11, where the process and the controller have the transfer functions

$$P(s) = \frac{1}{s+1}, \qquad C(s) = \frac{5(s+1)}{s}.$$

Notice that the process pole $s = -1$ is canceled by the zero of the controller. Derive the transfer functions G_{yv}, G_{yw}, G_{uv}, and G_{uw}. Compute the Kalman decomposition of a realization of the closed loop system with one state chosen as the process state and the other as the controller (integrator) state.

a) Discuss reachability with respect to the inputs v and w and observability from the signals y and u.

b) Discuss relations between pole/zero cancellations and the Kalman decomposition.

13.15 (AFM nanopositioning system) Consider the design in Example 13.11 and explore the effects of changing parameters α_0 and ζ_0.

13.16 (H_∞ control) Consider the matrix $H(P,C)$ in equation (13.32). Show that it has the singular values

$$\sigma_1 = 0, \qquad \sigma_2 = \bar{\sigma} = \sup_\omega \frac{\sqrt{(1+|P(i\omega)|^2)(1+|C(i\omega)|^2)}}{|1+P(i\omega)C(i\omega)|} = \|H(P,C))\|_\infty.$$

Also show that $\bar{\sigma} = 1/\delta_\nu(P, -1/C)$, which implies that $1/\bar{\sigma}$ is a generalization of the closest distance of the Nyquist plot to the critical point.

13.17 (Necessity of checking robustness) Consider the system

$$\frac{dx}{dt} = Ax + Bu = \begin{pmatrix} -1 & 0 \\ 1 & 0 \end{pmatrix} x + \begin{pmatrix} a-1 \\ 1 \end{pmatrix} u, \qquad y = Cx = \begin{pmatrix} 0 & 1 \end{pmatrix} x,$$

with $a = 1.25$. In Exercise 7.9 we designed a state feedback that gave the characteristic polynomial $\det(sI - BK) = s^2 + 2\zeta_c\omega_c s + \omega_c^2$ and in Exercise 8.6 we designed an observer with the characteristic polynomial $\det(sI - LC) = s^2 + 2\zeta_o\omega_o s + \omega_o^2$. The numerical values used were $a = 1.25$, $\omega_c = 5$, $\zeta_c = 0.6$, $\omega_o = 10$, and $\zeta_o = 0.6$. Compute the eigenvalues of the nominal system and the perturbed system where the process gain is increased by 2%. Also compute the loop transfer function and the sensitivity functions. Is there a way to know beforehand that the system will be highly sensitive?

13.18 (Disturbance weighting) Consider an H_∞ control problem with the disturbance weight W ($\overline{P} = PW$ and $\overline{C} = W^{-1}C$). Show that

$$\|\mathcal{G}(\overline{P}, \overline{C})\|_\infty \geq \sup_\omega \big(|S(i\omega)| + |T(i\omega)|\big).$$